Int J Adv Manuf Technol (2015) 79:1581–1595
DOI 10.1007/s00170-015-6881-0

ORIGINAL ARTICLE

Thermal simulation modeling of a hydrostatic machine feed platform

Teng Liu · Weiguo Gao · Yanling Tian · Ken Mao · Gaoxing Pan · Dawei Zhang

Received: 29 April 2014 / Accepted: 5 February 2015 / Published online: 6 March 2015

Abstract Hydrostatic guideways are widely applied into precision and ultra-precision machine tools. Meanwhile, the oil film heat transfer causes thermal disturbance to the machine accuracy. Therefore, it is necessary to study the mechanism of the oil film heat transfer and the heat-transfer-reducing method to improve the machine accuracy. This paper describes a comprehensive thermal finite element (FE) simulation modeling method for the hydrostatic machine feed platform to study methods of reducing machine thermal errors. First of all, the generating heat power of viscous hydraulic oil flowing between parallel planes is calculated based on the Bernoulli equation. This calculation is then employed for the simulation load calculations for the closed hydrostatic guideways, which is adopted by the hydrostatic machine feed platform. Especially, in these load calculations, the changing of oil film thickness (resulted from external loads) and the changing of oil dynamic viscosity (influenced by its temperature) are taken into account. Based on these loads, thermal FE simulation modeling of the hydrostatic machine feed platform is completed to predict and analyze its thermal characteristics. The reliability of this simulation modeling method is verified by experiments. The studies demonstrate that the hydrostatic machine thermal error degree is determined by the oil film heat transfer scale, and this scale is mainly influenced by the relative oil supply temperature to ambient temperature (quantitative comparison of oil supply temperature and ambient temperature). Furthermore, the reduction of the absolute value of this relative oil supply temperature can reduce the oil film heat transfer scale and improve the machine accuracy.

Keywords Thermal simulation modeling · Hydrostatic machine feed platform · Closed hydrostatic guideways · FE · Thermal errors

Nomenclature

W	Width of parallel planes (m)
L	Length of parallel planes (m)
h	Clearance between parallel planes (m)
P_{in}/P_{ou}	Pressures of viscous hydraulic oil at input/output sides of parallel planes (Pa)
P	Pressure of flow viscous hydraulic oil (Pa)
u	Velocity of flow viscous hydraulic oil (m/s)
t	Moment (s)
g	Acceleration due to gravity (m/s^2)
m	Mass of slide (kg)
ρ	Density of hydraulic oil (kg/m^3)
h_w	Friction power in 1 N gravity of oil film (m)
η_t	Average dynamic viscosity of hydraulic oil at a moment t (Pa s)
$\eta_0(T_0)$	Dynamic viscosity of hydraulic oil when its temperature is T_0 (Pa s)
P_S	Supply pressure of hydraulic oil (Pa)
T_S	Supply temperature of hydraulic oil (°C)
Q_t	Volume flow rate of hydraulic oil (m^3/s)
Q_{t_1}/Q_{t_2}	Volume flow rate of oil films of pad 1/2 (m^3/s)
Q_{G_1}/Q_{G_2}	Volume flow rate of oil film on gap restrictor of pad 1/2 (m^3/s)

T. Liu · W. Gao (✉) · Y. Tian · G. Pan · D. Zhang
Key Laboratory of Mechanism Theory and Equipment Design of Ministry of Education, Tianjin University, Tianjin 300072, China
e-mail: gaowg@tju.edu.cn

W. Gao · Y. Tian · K. Mao
School of Engineering, University of Warwick, Coventry CV4 7AL, UK

G. Pan
Tianjin No. 2 Machine Tool Co., Ltd., Tianjin 300409, China

Q_{L_1}/Q_{L_2}	Volume flow rate of oil film on land of pad 1/2 (m^3/s)
H_t	Heat generated by friction power of oil films (J/s)
H_{t_1}/H_{t_2}	Heat generated by friction power of oil films of pad 1/2 (J/s)
$H_{t\_up}/H_{t\_low}/H_{t\_hor}$	Heat generated by friction power of oil films of upper/lower/horizontal pad (J/s)
H_{G_1}/H_{G_2}	Heat generated by friction power of oil film on gap restrictor of pad 1/2 (J/s)
H_{L_1}/H_{L_2}	Heat generated by friction power of oil film on land of pad 1/2 (J/s)
A_e	Effective bearing area of hydrostatic pad (m^2)
E	External load (N)
E_V/E_H	External load on vertical/horizontal direction (N)
ε ($1>\varepsilon\geq 0$)	Relative displacement of oil film
$\varepsilon_V/\varepsilon_H$ ($1>\varepsilon_V\geq 0$, $1>\varepsilon_H\geq 0$)	Relative displacement of vertical/horizontal oil films
β	Design pressure ratio of hydrostatic pad
β_1/β_2	Pressure ratio of hydrostatic pad 1/2
P_{R_1} ($=P_S/\beta_1$)/P_{R_2} ($=P_S/\beta_2$)	Recess pressure of hydrostatic pad 1/2 (Pa)
h_0	Design thickness of oil films (m)
$F_1(=P_{R\_1}A_e)/F_2(=P_{R\_2}A_e)$	Reaction force from pad 1/2 (N)
L_G/W_G	Length/width of gap restrictor (m)
L_L	Radial scale of land (m)
W_L	Average circumferential scale of land (m)
M_{t_1}/M_{t_2}	Mass flow rate of oil films of pad 1/2 (kg/s)
$M_{t\_up}/M_{t\_low}/M_{t\_hor}$	Mass flow rate of oil films of upper/lower/horizontal pad (kg/s)
J_1/J_2	Stiffness of oil films of pad 1/2 (N/m)
$J_{up}/J_{low}/J_{hor}$	Stiffness of oil films of upper/lower/horizontal pad (N/m)
γ	V-T index coefficient
T	Temperature of hydraulic oil (°C)
$T_{out(t)}$	Output oil temperature of hydrostatic pad at moment t (°C)
$T_{out\_up(t)}$ /$T_{out\_low(t)}$/$T_{out\_hor(t)}$	Output oil temperature of upper/lower/horizontal hydrostatic pad at a moment t (°C)
ρ_M	Density of metal material of machine (kg/m^3)
k_M	Thermal conductivity of metal material of machine (w/(m K))
c_M	Specific heat of metal material of machine (J/(kg K))
J_M	Stiffness of metal material of machine (N/m)
μ	Poisson's ratio of metal material of machine
α	Linear expansion coefficient of metal material of machine
c	Specific heat of hydraulic oil (J/(kg K))
$T_{PA}/T_{PB}/T_{PC}/T_{PD}$	Measured temperature of positions A–D (°C)
T_{out}	Output temperature of hydraulic oil (°C)
$\Delta T_1/\Delta T_2/\Delta T_3$	Temperature gradient from oil films to environment in condition 1/2/3 (°C)
T_A	Ambient temperature (°C)
t_T/t_S	Total time/substep time length in transient FE simulation (min)
$\Delta_X/\Delta_Y/\Delta_Z$	Machine feed errors on $X/Y/Z$ direction (X: positioning error; Y/Z: straightness error)
$\delta_X/\delta_Y/\delta_Z$	Machine feed angle errors around $X/Y/Z$ direction
d	Distance of the two parallel lines in Fig. 16
α	Angle of two parallel lines and X-axis in Fig. 16

1 Introduction

Past decades have witnessed an increasingly widespread application of hydrostatic guideways or bearings into various kinds of high- and ultra-precision machine tools, owing to their special advantages [1]. These advantages include zero starting friction, low viscous running friction, high load-carrying capacity, high stiffness, high positioning accuracy, and so on [2]. Nevertheless, when the hydrostatic machine is working, the convective heat transfer exists between the oil films and the surface of machine metal material, and causes machine thermal errors. Therefore, the thermal simulation modeling investigation and the heat transfer reduction of the hydrostatic guideways or bearings can contribute to the accuracy improvement of the hydrostatic machine tools.

The thermal modeling method is the critical basis for the research on thermal characteristics and regulations of the hydrostatic guideways or bearings. A variety of researching efforts about this topic were based on experimental modeling methods. Yang et al. [3] studied the thermal effects in liquid oxygen hydrostatic journal bearings experimentally. Sharma et al. [4, 5] measured and summarized the influence of oil temperature rise on the symmetric and asymmetric slot-entry hybrid journal bearing, as well as the influence of oil temperature rise and bush deformation on static and dynamic performances of hole-entry hybrid journal bearing. Park et al. [6] investigated the relationship between oil temperature and positioning error of hydrostatic guideways by experimental methods. Kumar et al. [7] explored the influence of oil

temperature rise and bush deformation on the stability margin of hybrid journal bearing by experimental methods. Suzuki et al. [8] compared and analyzed two types of thermal deformations of the high-precision machine tool equipped with oil-lubricated hydrostatic bearings based on experiments. These experimental modeling activities are of great value onto the recognition about thermal characteristics of hydrostatic guideways or bearings. However, they are lacking in the discussions about hydrostatic heat transfer mechanism and then difficult to be used to predict and analyze thermal characteristics of hydrostatic guideways or bearings, during the design phase of hydrostatic machine tools.

Some other activities placed emphasis on theoretical and simulation modeling methods for thermal characteristics of hydrostatic guideways and bearings. Kapur and Verma [9] investigated the simultaneous inertia and temperature effects on the model of parallel stepped hydrostatic thrust bearing and obtained the expressions for pressure profile and load capacity under the conditions of the adiabatic flow. Sun et al. [10] studied the steady temperature field of double rows and narrow cavity hydrostatic and hydrodynamic hybrid bearings based on the adiabatic assumption and THD analysis. Zhang and Chi [11] adopted the finite difference method to overcome the simultaneous general Reynolds equation, energy equation and bearing thermal conductivity equation, analyzed theoretically the temperature field of the shallow recess step hydrostatic and hydrodynamic bearing. Zhang and Yuan [12] calculated the correlation between the pressure, temperature of hydraulic oil, and its turbulence, density, viscosity about the hydrostatic and hydrodynamic hybrid bearing with a capillary restrictor and four recesses. Fu and Zhu [13] established the three-dimensional temperature field model of hydrodynamic bearing, with the heat flux continuity condition, by the simultaneous solution of the generalized Reynolds equation, three-dimensional energy equations, three-dimensional heat transfer equation, and force equilibrium equation. Chen et al. [14] studied the thermal deformation effect of a hydrostatic spindle onto its oil films thickness, stiffness, load capacity, and machine accuracy, by a thermomechanical finite element (FE) model. Jiang et al. [15] analyzed thermal deformation influence to the machine accuracy of high-speed moving guide under different conditions by FE simulation method. Wang et al. [16] estimated the power consumption of hydrostatic guideways in working process and analyze the influence from its thermal deformation to machine accuracy by FE simulation method. Su et al. [17] established a hydrostatic spindle system model by FVEM and then studied the variation of its predicted thermal behaviors. These studies tried to establish mechanism models to analyze the thermal characteristics of hydrostatic guideways or bearings. But in these models, the hydrostatic heat transfer was always ignored or simplified to be constant values, which reduced their modeling accuracy. The heat transfer variation of hydrostatic guideways or bearings and its association with working conditions (such as oil supply temperature and ambient temperature) can hardly be studied based on them.

This paper presents a thermal FE simulation modeling method of a hydrostatic machine feed platform to analyze its thermal characteristics. This method considers the heat transfer of oil films to be related to the relative oil supply temperature to ambient temperature, and this heat transfer scale leads to the machine thermal error. The structure of this paper is arranged as follows: Section 2 introduces the necessary theory preparations of the thermal simulation modeling procedure for the hydrostatic machine feed platform. The discussed heat modeling of viscous hydraulic oil flowing between parallel planes is applied onto the required simulation load calculations. Then, based on these loads, in Section 3, thermal FE simulation modeling of hydrostatic machine feed platform is realized under various working conditions. In Section 4, the reliability of this FE simulation modeling method of hydrostatic machine feed platform is verified by experimental method. Furthermore, based on the simulation modeling results, Section 5 analyzes systemically the association between thermal errors of hydrostatic machine feed platform and its working condition (oil supply temperature and ambient temperature). Eventually, conclusions of the paper are summarized in Section 6.

2 Theory analyses for thermal simulation modeling of hydrostatic machine feed platform

This section discusses the theory preparations for the thermal FE simulation modeling method of the hydrostatic machine feed platform. Figure 1 depicts the logical relationships of these theory preparations: The necessary calculated loads for the thermal simulation modeling of hydrostatic machine feed platform includes mass flow rate, friction power, and stiffness of oil films. These calculations consider the changing of oil

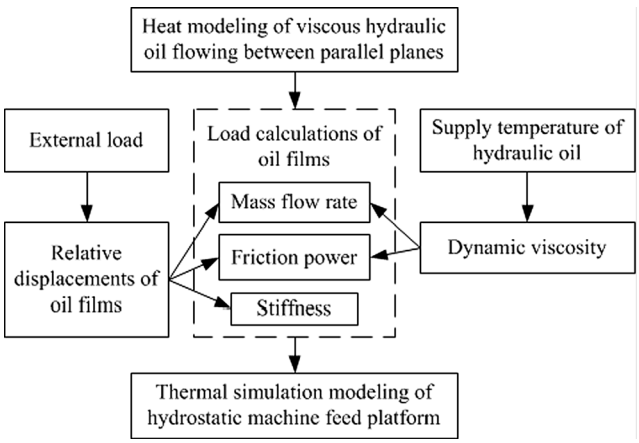

Fig. 1 Theory analyses for thermal simulation modeling of hydrostatic machine feed platform

film thickness (resulted from external loads) and the changing of oil dynamic viscosity (influenced by its supply temperature), and they are guided by the heat modeling of viscous hydraulic oil flowing between parallel planes. The thermal FE simulation modeling of hydrostatic machine feed platform will be completed based on these calculated loads. The calculation methods are deduced as follows.

2.1 Heat modeling of viscous hydraulic oil flowing between parallel planes

The theory analyses about the oil films of hydrostatic guideways must be based on a heat modeling of friction power generated by viscous hydraulic oil flowing between parallel planes. This modeling is described in Fig. 2: The viscous hydraulic oil has a laminar flow on X direction between fixed parallel planes 1 and 2. Parallel planes have the same width W, same length L, and a clearance h ($L \gg h$, $W \gg h$). The pressure values of the flowing viscous hydraulic oil at input and output sides of parallel planes are P_{in} and P_{ou} respectively ($P_{in} > P_{ou}$). $L \gg h$ and $W \gg h$ mean that the flowing viscous hydraulic oil has the approximately uniform temperature and pressure distributions on Y and Z directions. Thus, with the potential energy of flowing viscous hydraulic oil being ignored, the Bernoulli equation for viscous liquid at a moment t is:

$$\frac{P_{in}}{\rho g} + \frac{u^2}{2g} = \frac{\left(P_{in} + \frac{dP}{dx}L\right)}{\rho g} + \frac{\left(u + \frac{du}{dx}L\right)^2}{2g} + h_w \tag{1}$$

The laminar flow means $du/dx=0$, which presents the uniform flow velocity of viscous hydraulic oil on X direction. Thus, Eq. (1) can be simplified by $du/dx=0$ as follows:

$$\frac{L}{\rho g} \bullet \frac{dP}{dx} + h_w = 0 \tag{2}$$

Besides, there is a linear pressure decline of the flow viscosity hydraulic oil on X direction, which means:

$$\frac{dP}{dx} = \frac{P_{ou} - P_{in}}{L} \tag{3}$$

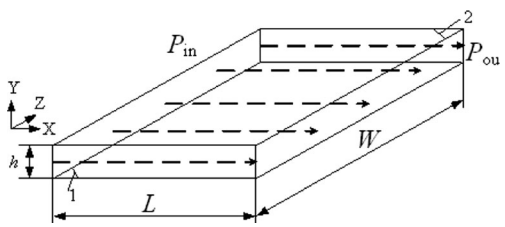

Fig. 2 Flowing viscous hydraulic oil between parallel planes

Substituting Eq. (3) into Eq. (2):

$$h_w = \frac{1}{\rho g}(P_{in} - P_{ou}) \tag{4}$$

The volume flow rate Q_t at the moment t is [18]:

$$Q_t = \frac{Wh^3}{12\eta_t L}(P_{in} - P_{ou}) \tag{5}$$

Then, the heat generated by friction power of the flowing viscous hydraulic oil at the moment t can be expressed as:

$$H_t = h_w \rho g Q_t \tag{6}$$

Substituting Eqs. (4) and (5) into Eq. (6), the friction power H_t of the flowing viscous hydraulic oil at the moment t is:

$$H_t = \frac{Wh^3}{12\eta_t L}(P_{in} - P_{ou})^2 \tag{7}$$

The conclusions of this subsection are preparations and guidance for simulation load calculations of closed hydrostatic guideways with gap restrictors.

2.2 Simulation load calculations of closed hydrostatic guideways with gap restrictors considering the variation of oil film thickness

2.2.1 Operational principle of closed hydrostatic guideways with gap restrictors

The structure of the single pad of closed hydrostatic guideways with gap restrictors is shown in the axonometric drawing Fig. 3a, and Fig. 3b is an orthography drawing of gap restrictors and land, especially the average circumferential length W_L of the land is shown as a dash and dot line and has a middle position between the inner and outer edges of land. Meanwhile, the effective bearing area A_e of the hydrostatic pad is the area surrounded by the dash and dot line in Fig. 3b.

The operational principle of the closed hydrostatic guideways with gap restrictors is shown in Fig. 4. This figure illustrates the hydrostatic pad 1(2) to be a view of cross-section A–A of Fig. 3b: When the pump is switched on, the pressurized hydraulic oil is conveyed from oil supply hole into hydrostatic pad 1(2). It flows into clearances between bilateral gap restrictors and guide rail to form oil films in them, and be directed by oil output holes into internal pipelines, then be collected by oil input hole of the opposite pad 2(1) into its recess. Finally, it flows into the clearance between land and guide rail to form the oil film and goes into the oil returning chute. If an external load E is exerted on the closed hydrostatic guideways with gap restrictors, the oil film thickness values of

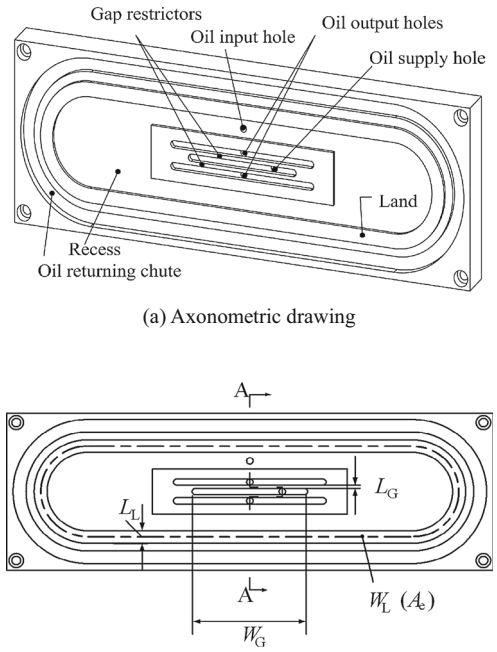

(a) Axonometric drawing

(b) Vertical projection

Fig. 3 A single pad of closed hydrostatic guideways with gap restrictors. **a** Axonometric drawing. **b** Vertical projection

hydrostatic pads 1 and 2 will be $h_0+\varepsilon h_0$ and $h_0-\varepsilon h_0$, respectively.

The thickness scale of oil films is far less than its length and width, so that the oil films have the indelible friction power, decreasing oil pressure and increasing oil temperature. Generally, the friction power results from two contributions: One part is the friction power of the hydraulic power supplied by the pump through the restrictors and land to drive the laminar flow in oil films; another is the friction power in the shear flow generated by the relative motion of hydrostatic guideways [14]. In this paper, the latter part is ignored, for the reason that closed hydrostatic guideways have a low speed to the machine when they are working [19]. To sum up, the conclusions in Section 2.1 will be used to analyze the mass flow rate, friction power and stiffness of oil films, which are required by the thermal FE simulation modeling of the closed hydrostatic guideways with gap restrictors.

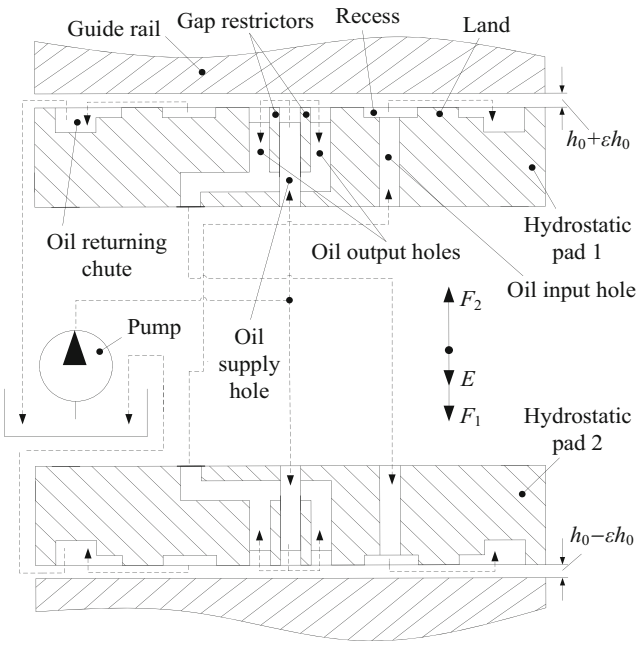

Fig. 4 Operational principle of closed hydrostatic guideways with gap restrictors

2.2.2 Mass flow rate of oil films

According to Eq. (5), the volume flow rates of oil films on unilateral gap restrictor and land of pads 1 and 2 at a moment t respectively are:

$$Q_{G_1} = \frac{W_G(h_0+\varepsilon h_0)^3}{12\eta_t L_G}(P_S - P_{R_2}) = \frac{W_G(h_0+\varepsilon h_0)}{12\eta_t L_G}\left(P_S - \frac{P_S}{\beta_2}\right) \quad (8)$$

$$Q_{G_2} = \frac{W_G(h_0-\varepsilon h_0)^3}{12\eta_t L_G}(P_S - P_{R_1}) = \frac{W_G(h_0-\varepsilon h_0)^3}{12\eta_t L_G}\left(P_S - \frac{P_S}{\beta_1}\right) \quad (9)$$

$$Q_{L_2} = \frac{W_L(h_0-\varepsilon h_0)^3}{12\eta_t L_L}(P_{R_2} - 0) = \frac{W_L(h_0-\varepsilon h_0)^3}{12\eta_t L_L}\left(\frac{P_S}{\beta_1} - 0\right) \quad (10)$$

$$Q_{L_2} = \frac{W_L(h_0-\varepsilon h_0)^3}{12\eta_t L_L}(P_{R_2} - 0) = \frac{W_L(h_0-\varepsilon h_0)^3}{12\eta_t L_L}\left(\frac{P_S}{\beta_2} - 0\right) \quad (11)$$

The continuity of the volume flow rates of oil films on bilateral gap restrictors and land of pads 1 and 2 at a moment t are:

$$Q_{t_1} = 2Q_{G_2} = Q_{L_1} = \frac{W_G(h_0-\varepsilon h_0)^3}{6\eta_t L_G}\left(P_S - \frac{P_S}{\beta_1}\right) = \frac{W_L(h_0+\varepsilon h_0)^3}{12\eta_t L_L}\left(\frac{P_S}{\beta_1} - 0\right) \quad (12)$$

$$Q_{t_2} = 2Q_{G_1} = Q_{L_2} = \frac{W_G(h_0+\varepsilon h_0)^3}{6\eta_t L_G}\left(P_S - \frac{P_S}{\beta_2}\right) = \frac{W_L(h_0-\varepsilon h_0)^3}{12\eta_t L_L}\left(\frac{P_S}{\beta_2} - 0\right) \quad (13)$$

Equations (12) and (13) can be arranged into:

$$\beta_1 = \frac{L_G W_L (1+\varepsilon)^3}{2L_L W_G (1-\varepsilon)^3} + 1 \tag{14}$$

$$\beta_2 = \frac{L_G W_L (1-\varepsilon)^3}{2L_L W_G (1+\varepsilon)^3} + 1 \tag{15}$$

As far as Eqs. (14) and (15) are concerned, when the external load $E=0$, $\varepsilon=0$ and $\beta=\beta_1=\beta_2$. Thus:

$$\beta = \beta_1|_{\varepsilon=0} = \beta_2|_{\varepsilon=0} = \frac{W_L L_G}{2W_G L_L} + 1 \tag{16}$$

In order to find out the relationships between pressure ratios of hydrostatic pads β_1/β_2 ($1>\varepsilon>0$), the design pressure ratio of these hydrostatic pad β ($\varepsilon=0$) and the relative displacement of oil film ε, Eq. (16) is substituted into Eqs. (14) and (15), respectively, to offset their common term $L_G W_L / 2L_L W_G$:

$$\beta_1 = (\beta-1)\frac{(1+\varepsilon)^3}{(1-\varepsilon)^3} + 1 \tag{17}$$

$$\beta_2 = (\beta-1)\frac{(1-\varepsilon)^3}{(1+\varepsilon)^3} + 1 \tag{18}$$

Thus, according to Eqs. (12) and (13), the mass flow rates of oil films of pads 1 and 2 at a moment t, respectively, are:

$$M_{t_1} = \rho Q_{t_1} = \frac{\rho P_S W_G (\beta-1)(h_0+\varepsilon h_0)^3}{6\eta_t L_G \left[(\beta-1)\frac{(1+\varepsilon)^3}{(1-\varepsilon)^3}+1\right]} = \frac{\rho P_S W_L (h_0+\varepsilon h_0)^3}{12\eta_t L_L \left[(\beta-1)\frac{(1+\varepsilon)^3}{(1-\varepsilon)^3}+1\right]} \tag{19}$$

$$M_{t_2} = \rho Q_{t_2} = \frac{\rho P_S W_G (\beta-1)(h_0-\varepsilon h_0)^3}{6\eta_t L_G \left[(\beta-1)\frac{(1-\varepsilon)^3}{(1+\varepsilon)^3}+1\right]} = \frac{\rho P_S W_L (h_0-\varepsilon h_0)^3}{12\eta_t L_L \left[(\beta-1)\frac{(1-\varepsilon)^3}{(1+\varepsilon)^3}+1\right]} \tag{20}$$

2.2.3 Heat generated by friction power of oil films

According to Eq. (7), the heat values generated by friction powers of the oil films on unilateral gap restrictor and land of pads 1 and 2 at a moment t, respectively, are:

$$H_{G_1} = \frac{W_G (h_0+\varepsilon h_0)^3}{12\eta_t L_G}(P_S - P_{R_2})^2 = \frac{W_G (h_0+\varepsilon h_0)^3}{12\eta_t L_G}\left(P_S - \frac{P_S}{\beta_2}\right)^2 \tag{21}$$

$$H_{G_2} = \frac{W_G (h_0+\varepsilon h_0)^3}{12\eta_t L_G}(P_S - P_{R_1})^2 = \frac{W_G (h_0+\varepsilon h_0)^3}{12\eta_t L_G}\left(P_S - \frac{P_S}{\beta_1}\right)^2 \tag{22}$$

$$H_{L_1} = \frac{W_G (h_0+\varepsilon h_0)^3}{12\eta_t L_L}(P_{R_1} - 0)^2 = \frac{W_L (h_0+\varepsilon h_0)^3}{12\eta_t L_L}\left(\frac{P_S}{\beta_1}\right)^2 \tag{23}$$

$$H_{L_2} = \frac{W_L (h_0+\varepsilon h_0)^3}{12\eta_t L_L}(P_{R_2} - 0)^2 = \frac{W_L (h_0+\varepsilon h_0)^3}{12\eta_t L_L}\left(\frac{P_S}{\beta_2}\right)^2 \tag{24}$$

Because there are two oil films being on the bilateral gap restrictors and one oil film being on the land in each hydrostatic pad, the heat generated by friction powers of oil films in pads 1 and 2 at a moment t are, respectively:

$$H_{t_1} = 2H_{G_1} + H_{L_1} = \frac{{P_S}^2 (h_0+\varepsilon h_0)^3}{6\eta_t}\left[\frac{W_G}{L_G}\left(1-\frac{1}{\beta_2}\right)^2 + \frac{W_L}{2L_L}\left(\frac{1}{\beta_1}\right)^2\right] \tag{25}$$

$$H_{t_2} = 2H_{G_2} + H_{L_2} = \frac{{P_S}^2 (h_0-\varepsilon h_0)^3}{6\eta_t}\left[\frac{W_G}{L_G}\left(1-\frac{1}{\beta_1}\right)^2 + \frac{W_L}{2L_L}\left(\frac{1}{\beta_2}\right)^2\right] \tag{26}$$

Substituting Eqs. (17) and (18) into Eqs. (25) and (26), respectively, the heat values generated by friction powers of oil films can be rewritten as follows:

$$H_{t_1} = \frac{{P_S}^2}{6\eta_t}\left\{\frac{W_G(\beta-1)^2(1-\varepsilon)^3(h_0-\varepsilon h_0)^3}{L_G(1+\varepsilon)^3\left[(\beta-1)\frac{(1-\varepsilon)^3}{(1+\varepsilon)^3}+1\right]^2} + \frac{W_L(h_0+\varepsilon h_0)^3}{2L_L\left[(\beta-1)\frac{(1+\varepsilon)^3}{(1-\varepsilon)^3}+1\right]^2}\right\} \tag{27}$$

$$H_{t_2} = \frac{{P_S}^2}{6\eta_t}\left\{\frac{W_G(\beta-1)^2(1+\varepsilon)^3(h_0+\varepsilon h_0)^3}{L_G(1-\varepsilon)^3\left[(\beta-1)\frac{(1+\varepsilon)^3}{(1-\varepsilon)^3}+1\right]^2} + \frac{W_L(h_0-\varepsilon h_0)^3}{2L_L\left[(\beta-1)\frac{(1-\varepsilon)^3}{(1+\varepsilon)^3}+1\right]^2}\right\} \tag{28}$$

2.2.4 Stiffness of oil films

The stiffness values J_1 and J_2 of oil films of pads 1 and 2 are, respectively:

$$J_1 = \frac{\mathrm{d}F_1}{\mathrm{d}(h_0+\varepsilon h_0)} = \frac{1}{h_0}\frac{\mathrm{d}(P_{R_1}A_e)}{\mathrm{d}\varepsilon} = \frac{P_S A_e}{h_0}\frac{\mathrm{d}}{\mathrm{d}\varepsilon}\left(\frac{1}{\beta_1}\right) \quad (29)$$

$$J_2 = \frac{\mathrm{d}F_2}{\mathrm{d}(h_0+\varepsilon h_0)} = \frac{1}{h_0}\frac{\mathrm{d}(P_{R_2}A_e)}{\mathrm{d}\varepsilon} = \frac{P_S A_e}{h_0}\frac{\mathrm{d}}{\mathrm{d}\varepsilon}\left(\frac{1}{\beta_2}\right) \quad (30)$$

Substituting Eqs. (17) and (18) into Eqs. (29) and (30), the stiffness values of oil films of pads 1 and 2 can be achieved as follows:

$$J_1 = \frac{P_S A_e}{h_0}\frac{6(1-\beta)(\varepsilon^2-1)^2}{\left[\beta(\varepsilon+1)^3-2\varepsilon(3+\varepsilon^2)\right]^2} \quad (31)$$

$$J_2 = \frac{P_S A_e}{h_0}\frac{6(\beta-1)(\varepsilon^2-1)^2}{\left[\beta(\varepsilon-1)^3-2\varepsilon(3+\varepsilon^2)\right]^2} \quad (32)$$

2.2.5 Relative displacement of oil films

In all the equations above, the relative displacement ε must be obtained by the force–balance relationship about the closed hydrostatic guideways with gap restrictors shown in Fig. 4:

$$F_1 - F_2 + E = \frac{P_S}{\beta_1}A_e - \frac{P_S}{\beta_2}A_e + E = 0 \quad (33)$$

Substituting Eqs. (17) and (18) into Eq. (33), we obtain:

$$\frac{E}{P_S A_e} = \frac{1}{(\beta-1)\frac{1-3\varepsilon+3\varepsilon^2-\varepsilon^3}{1+3\varepsilon+3\varepsilon^2+\varepsilon^3}+1} - \frac{1}{(\beta-1)\frac{1+3\varepsilon+3\varepsilon^2+\varepsilon^3}{1-3\varepsilon+3\varepsilon^2-\varepsilon^3}+1} \quad (34)$$

The values of relative displacement ε can be obtained by solving Eq. (34), and the value of ε in the range of [0, 1) must be selected from the results, to be used into the calculations of mass flow rate, friction power and stiffness of oil films.

2.3 Simulation load calculations of hydrostatic machine feed platform

To calculate mass flow rate, friction power, and stiffness of oil films described in Section 2.2, the values of relative displacement and dynamic viscosity must be obtained by the following methods.

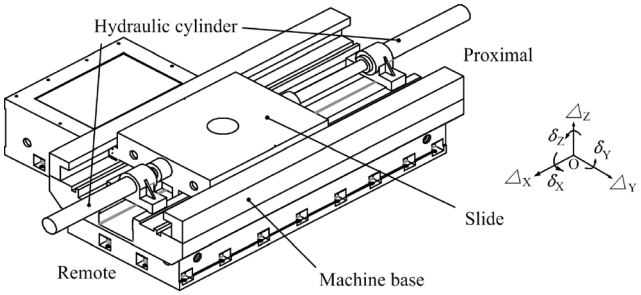

Fig. 5 Structure and six error kinds of hydrostatic machine feed platform

2.3.1 Relative displacement of oil films of hydrostatic machine feed platform

As illustrated in Fig. 5, the hydrostatic machine feed platform is assembled with a slide and a machine base, and the proximal and remote hydraulic cylinders can drive the slide collaboratively to realize its round-trip linear feed motion within a more than 1000 mm stroke. Being the horizontal feed axis of a hydrostatic machine tool, it has six machine feed axis error kinds: Δ_X, Δ_Y, Δ_Z, δ_X, δ_Y, and δ_Z [20].

All the sliding contacts between the slide and machine base are based on the closed hydrostatic guideways with gap restrictors. The layout of the hydrostatic pads is described specifically in Fig. 6: There are two pairs of horizontal hydrostatic pads and six pairs of vertical ones located at the slide.

The gravity of slide is sustained by six pairs of vertical hydrostatic pads, which is illustrated in Fig. 7. As far as one pair of vertical hydrostatic pads is concerned, $E_V = mg/6$, and thickness values of upper and lower vertical oil films are $h_0+\varepsilon_V h_0$ and $h_0-\varepsilon_V h_0$, respectively; the thickness values of horizontal hydrostatic pads remain h_0, for that $E_H = 0$.

Therefore, being the applications of the method provided by Section 2.2.5, the relative displacement of horizontal oil

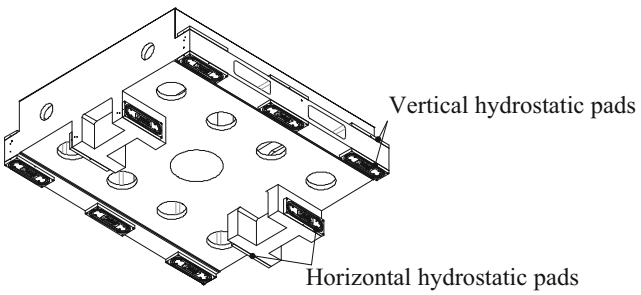

Fig. 6 Layout of hydrostatic pads on slide

films: $\varepsilon_H=0$, and the vertical one can be obtained by solving the following equation:

$$\frac{mg}{6P_S A_e}=\frac{1}{(\beta-1)\frac{1-3\varepsilon_V+3\varepsilon_V^2-\varepsilon_V^3}{1+3\varepsilon_V+3\varepsilon_V^2+\varepsilon_V^3}+1}-\frac{1}{(\beta-1)\frac{1+3\varepsilon_V+3\varepsilon_V^2+\varepsilon_V^3}{1-3\varepsilon_V+3\varepsilon_V^2-\varepsilon_V^3}+1} \tag{35}$$

Then, the real ε_V value must be determined by the selection from the results of Eq. (35), according to the range [0, 1).

2.3.2 Dynamic viscosity of oil films dependent on temperature

With the influence consideration from temperature factor onto oil dynamic viscosity, the Reynolds *V–T* equation [21] is used into the methods provided in Sections 2.2.2 and 2.2.3:

$$\eta=\eta_0 e^{-\gamma(T-T_0)} \tag{36}$$

Based on the Eq. (36) and for the feasibility of FE simulation method, the average dynamic viscosity value η_t of oil films in one pad at a moment t is approximately obtained as follows:

$$\eta_t=\begin{cases}\eta_0 e^{-\gamma(T_S-T_0)}, t=0\\ \eta_0 e^{-\gamma\left(\frac{T_S+T_{out(t-1)}}{2}-T_0\right)}, t>0\end{cases} \tag{37}$$

$T_{out(t-1)}$ stands for the output oil temperature of hydrostatic pad at the moment $t-1$. In transient FE simulation, this value can be automatically acquired from the result of every substep by APDL.

3 Thermal FE simulation modeling of hydrostatic machine feed platform

This section determines some design and process parameters of hydrostatic machine feed platform. Then its simulation loads can be obtained by the methods introduced in Section 2 to complete its FE simulation modeling. This section illustrates the realization of the thermal FE simulation modeling of the hydrostatic machine feed platform. This realization includes the determination of CAE modeling, simulation loads, and boundary conditions, and some necessary analyses about thermal FE simulation results.

Table 1 Design parameters of hydrostatic machine feed platform and its closed hydrostatic guideways with gap restrictors

Design parameters	Values
Mass of slide m (kg)	2.0582e3
Density of metal material of machine ρ_M (kg/m^3)	7350
Thermal conductivity of metal material of machine k_M (w/(m K))	35.7
Specific heat of metal material of machine c_M (J/(kg K))	460
Stiffness of metal material of machine J_M (N/m)	1.2e11
Poisson's ratio of metal material of machine μ	0.125
Linear expansion coefficient of metal material of machine α	10e−6
Design pressure ratio β	2
V–T index coefficient γ (used in Reynolds *V–T* equation)	0.468
Supply pressure of hydraulic oil P_S (Pa)	2.4e6
Design thickness of oil films h_0 (m)	2e−5
Density of hydraulic oil ρ (kg/m^3)	865
Specific heat of hydraulic oil c (J/(kg K))	2.1e3
Dynamic viscosity of hydraulic oil η (Pa s)	η_0=1.27e3 (T_0=20 °C)
Width of gap restrictor W_G (m)	2e−3
Length of gap restrictor L_G (m)	7e−2
Radial scale of land W_L (m)	8e−3
Average circumferential scale of land L_L (m)	0.6
Effective bearing area A_e (m^2)	3.9e−2

3.1 CAE modeling and determination of simulation loads and boundary conditions

The main design parameters of the hydrostatic machine feed platform and its closed hydrostatic guideways with gap restrictors are listed in Table 1. Based on these parameters, the simplified CAE model of the hydrostatic machine feed platform

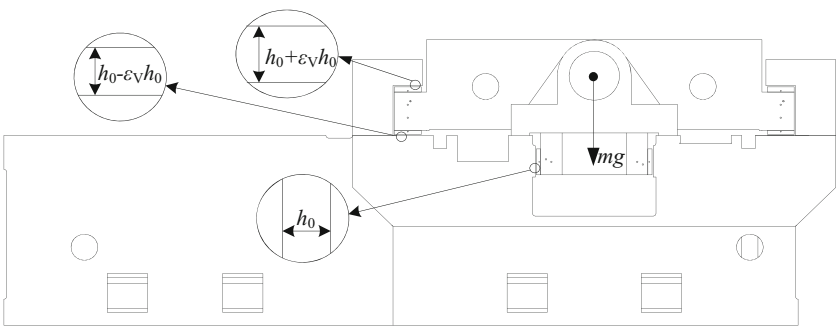

Fig. 7 Force analysis about slide

is established in ANSYS. The distance between the slide and the proximal of machine base varies from 0 to 1000 mm, and the increasing step is 200 mm. Therefore, the machine stroke is divided into five parts averagely to predict and analyze thermal errors of the hydrostatic machine feed platform.

As shown in Fig. 8, the sheet models are established to stand for oil films of hydrostatic pads. Then, the established models are meshed, and the 3-D thermal surface effect elements are created between oil film models and the machine model, in order to simulate the convective heat transfer between oil films and the machine in ANSYS. The local cylindrical coordinate system is built up based on every oil film model. It is built with the central location of oil film model being its origin and the perpendicular direction to the model being its Z axis. Then, the elements used to mesh oil film model are set abiding by this local cylindrical coordinate system. Thus, every oil film model is set to have a radial divergent outflow originated from oil supply location.

The values of mass flow rate, friction power, and stiffness of oil films are obtained by the methods provided in Section 2.2. Some fluid parameters in Table 1 and the friction power and stiffness obtained are set up for elements of every oil film model, and the metal material parameters in Table 1 are set up for elements of machine model. The oil supply temperature is exerted onto the oil supply location shown in Fig. 8. The mass flow rate of oil films must be exerted on the whole oil film model by a heat flux method in the FE simulation. Specially, the mass flow rates and friction powers must be exerted as functions (with moment t being the independent variable) for the transient FE simulation. In these functions, the values of $T_{\text{out\_up}(t-1)}$, $T_{\text{out\_low}(t-1)}$, and $T_{\text{out\_hor}(t-1)}$ are acquired automatically from edges of oil film models, shown in Fig. 8, after every substep. This procedure is realized by APDL in ANSYS, and the transient FE simulations are done in condition 1/2/3 (T_A=17 °C/20 °C/23 °C, T_S=20 °C), to respectively study thermal characteristics of hydrostatic machine feed platform. Finally, in all these simulation conditions, the three-dimensional displacement fix constraint is exerted to the bottom surface of the machine model, and the ambient temperature and gravity are exerted onto the machine model as a whole.

3.2 Results of FE simulations

This paper concentrates on the temperature and horizontal/vertical thermal deformation results of transient FE simulations about hydrostatic machine feed platform. Figures 9 and 10 show, respectively, its temperature and vertical thermal deformation fields of conditions 1–3 at typical simulation steps (the distance between the slide and the proximal of machine base is 600 mm). It can be seen from Fig. 9 that hydrostatic pads and their surrounding areas have higher temperature than other areas of the machine. With time increase, the temperature gradients are growingly obvious in all the three conditions. Meanwhile, the temperature gradients in condition 2 (T_A=T_S=20 °C) are likely to be less obvious than condition 1 (T_A<T_S) and condition 3 (T_A>T_S). On the other hand, the vertical deformations caused by oil film heat transfer of these

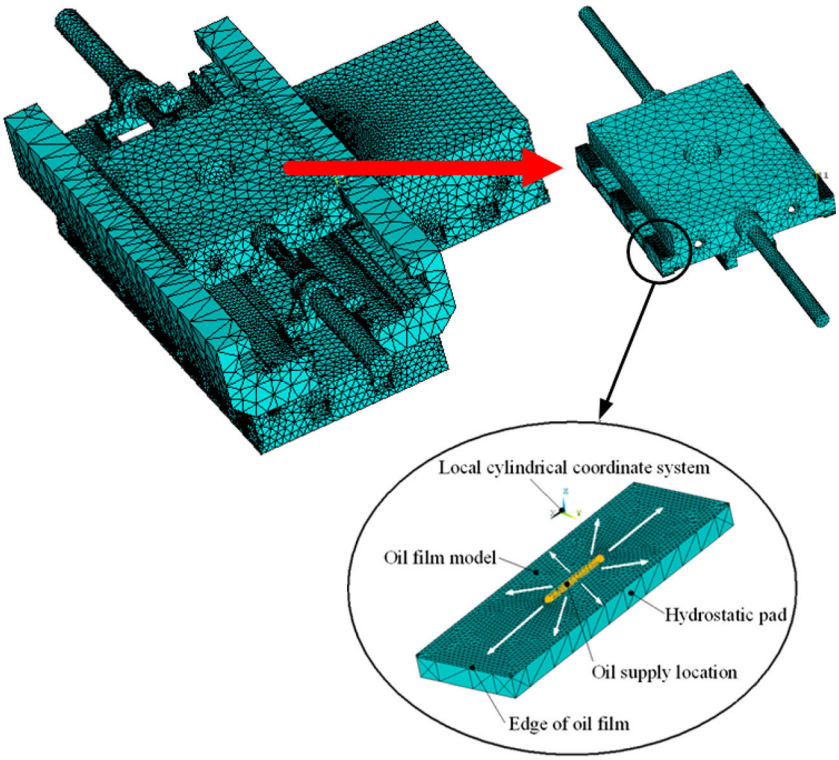

Fig. 8 Model meshing and determination of simulation loads and boundary conditions onto hydrostatic machine feed platform

three conditions are illustrated in Fig. 10: With time increase, thermal deformations have the growing tendency, and the machine thermal deformation degree in condition 2 is also lower than other two conditions. These thermal FE simulation results are the bases for the further discussions.

4 Experimental verifications

The reliability of the thermal FE simulation modeling method of hydrostatic machine feed platform is verified by experimental methods. These verifications are based on the condition 1/2/3 (T_A=17 °C/20 °C/23 °C, T_S=20 °C) defined above. This section introduces the experimental procedure and the comparisons of experimental and simulation results. These comparisons can lead to the reliability verification of the studied FE simulation modeling method.

4.1 Experimental procedure

As shown in Fig. 11, verification experiments were done by this method: When the hydrostatic machine feed platform was working at a low feeding velocity, temperatures and thermal deformations were continuously measured by thermal resisters

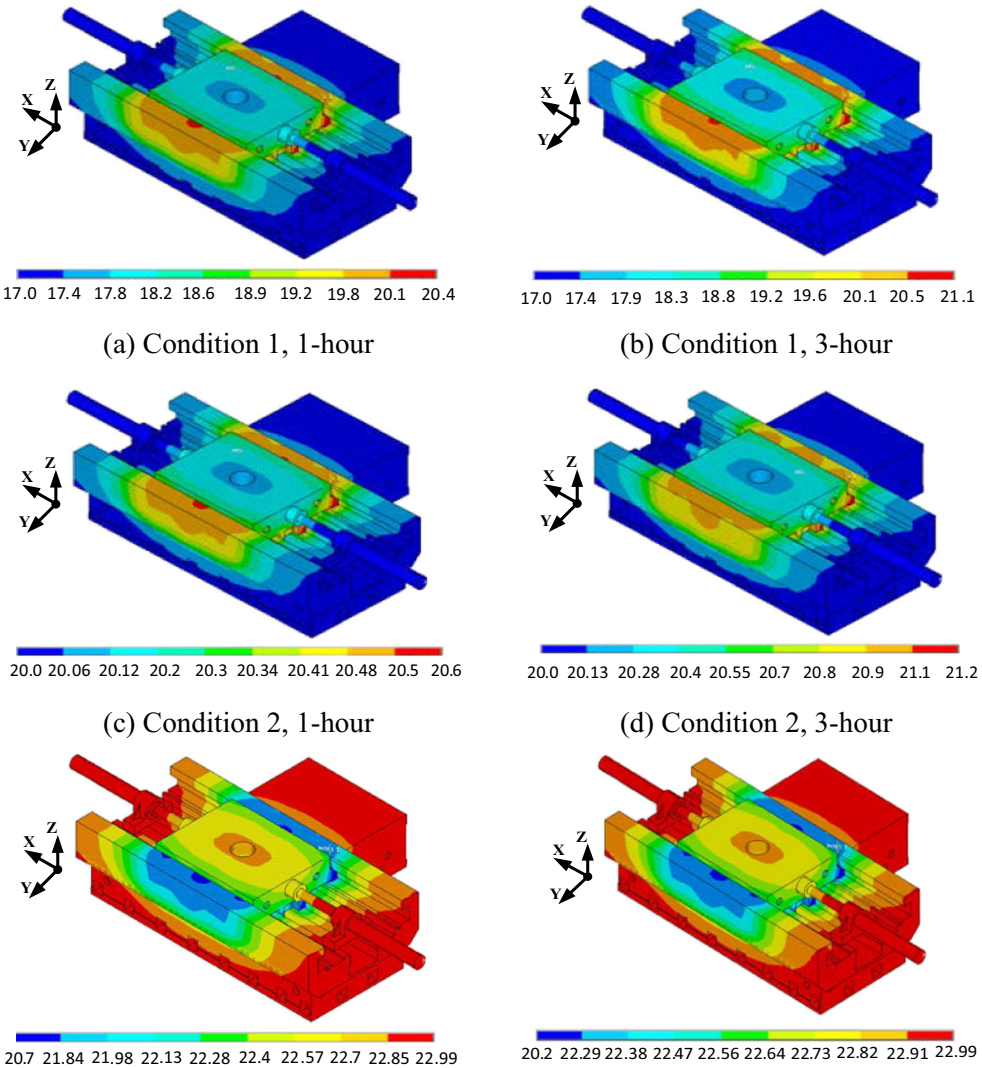

(a) Condition 1, 1-hour (b) Condition 1, 3-hour

(c) Condition 2, 1-hour (d) Condition 2, 3-hour

(e) Condition 3, 1-hour (f) Condition 3, 3-hour

Fig. 9 Temperature fields of hydrostatic machine feed platform

and the laser interferometer, respectively. The temperature signals from the former were conveyed by signal gathering system to the host computer, and thermal deformation values from the latter were directly received by the host computer.

Specially, the locations of sensors mentioned on the machine are also illustrated in Fig. 11: Thermal resisters are located to positions A–D; temperatures of positions A and B (T_{PA} and T_{PB}) stand for the oil film temperature; temperature of C (T_{PC}) is measured to be ambient temperature; and temperature of D (T_{PD}) corresponds to the oil output temperature of hydrostatic pads. On the other hand, the reflector of laser interferometer is located at position O, in order to measure the horizontal and vertical thermal deformations of the working slide. The setting method of the laser interferometer is shown in Fig. 12. Experiments were done in conditions 1–3 defined above (T_A=17 °C/20 °C/23 °C, T_S=20 °C), respectively, to verify comprehensively the thermal FE simulation modeling method of hydrostatic machine feed platform. The measurements in every defined condition would not be terminated until the changing scales of its signals in last hour were <15 % of the ones in first hour [22].

4.2 Comparisons between experimental data and simulation results

According to the locations A–D in Fig. 11, the simulated temperature values are obtained from the machine temperature fields of three defined conditions in Fig. 9. They are compared

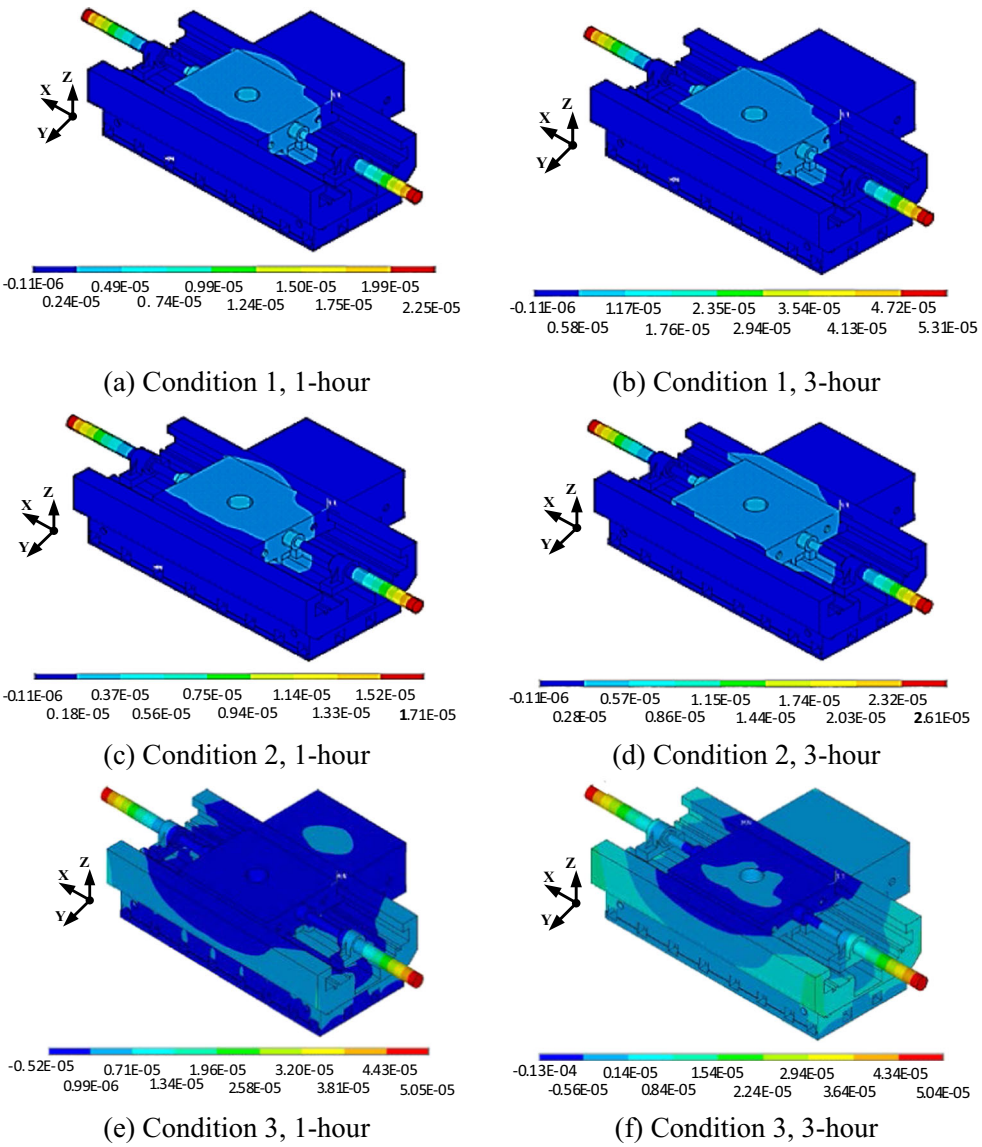

(a) Condition 1, 1-hour (b) Condition 1, 3-hour

(c) Condition 2, 1-hour (d) Condition 2, 3-hour

(e) Condition 3, 1-hour (f) Condition 3, 3-hour

Fig. 10 Vertical thermal deformation fields of hydrostatic machine feed platform

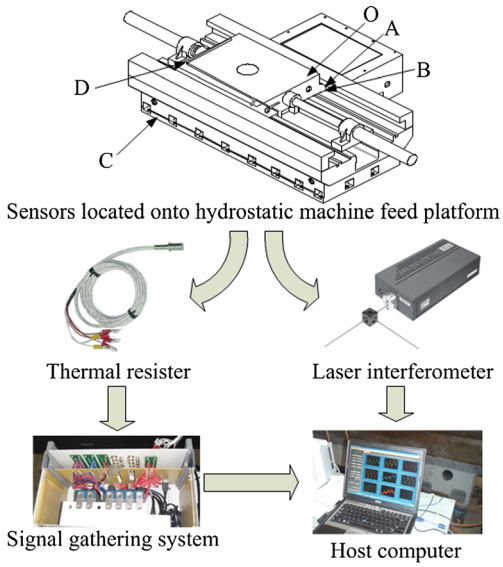

Fig. 11 Experimental method

with the measured T_{PA}–T_{PD} of three defined conditions, respectively, in Fig. 13. Meanwhile, thermal deformation values of location O (shown in Fig. 11) are obtained from the simulated machine thermal deformations in Fig. 10. Both the obtained horizontal (*Y* direction) and vertical (*Z* direction) thermal deformations are compared with the corresponding measured values of three defined conditions, respectively. Figure 14 shows the comparisons of the vertical simulated thermal deformations and their measured values. It can be clarified by Figs. 13 and 14 that the simulated results are in agreement with the corresponding experimental data in three defined conditions. These consistencies can verify the reliability of the introduced thermal FE simulation modeling method of hydrostatic machine feed platform.

5 Analyses and discussions

Some further analyses based on FE simulation results in Section 3 are done in this section. On the one hand, the oil film heat transfers in conditions 1–3 are analyzed and compared. The difference of them is the dominant factor causing

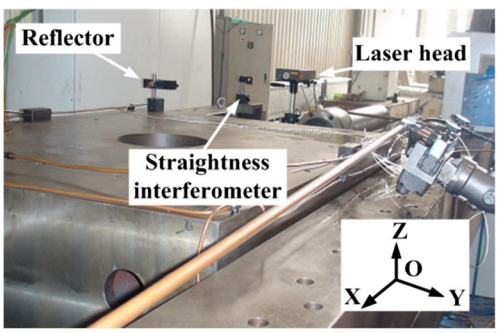

Fig. 12 Setting method of laser interferometer

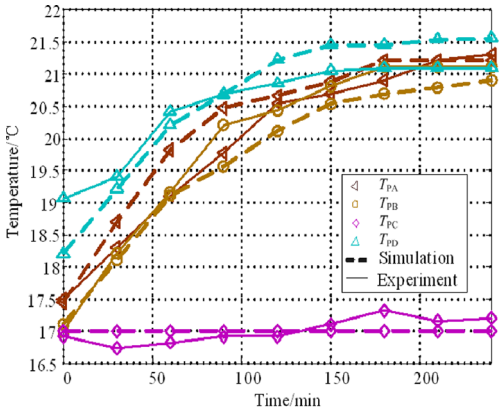

(a) Condition 1

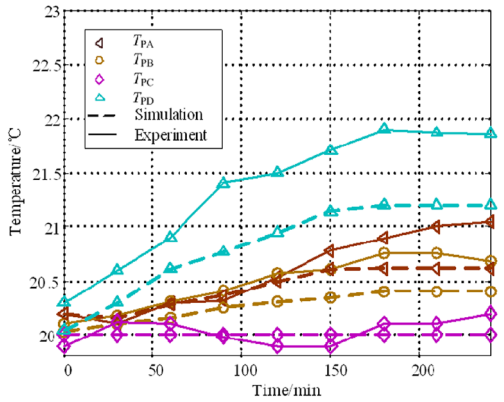

(b) Condition 2

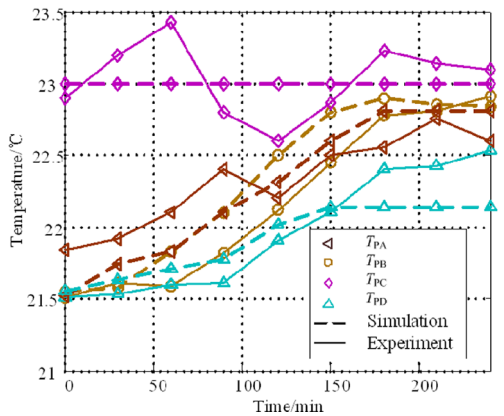

(c) Condition 3

Fig. 13 Temperature comparisons between experimental data and FE simulation results

thermal deformation difference of hydrostatic machine feed platform. On the other hand, thermal deformation FE results of the platform lead to its thermal error prediction methods. The association between the predicted machine thermal errors and the oil film heat transfer is analyzed and discussed.

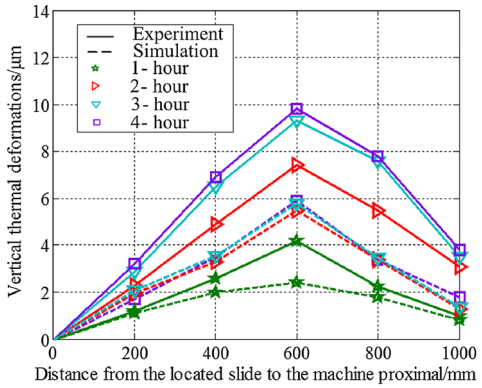

(a) Condition 1

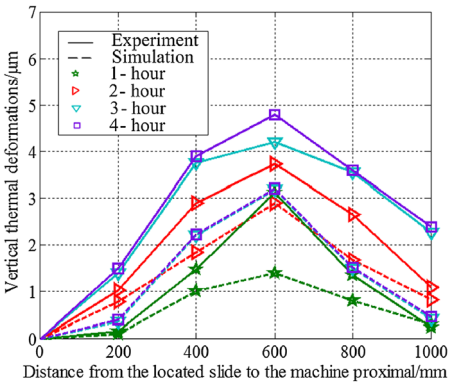

(b) Condition 2

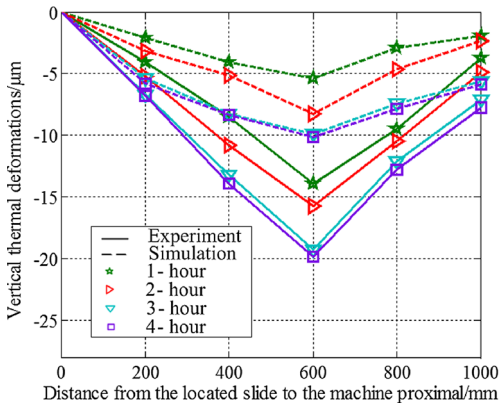

(c) Condition 3

Fig. 14 Vertical thermal deformation comparisons between experimental data and FE simulation results

5.1 Oil film heat transfer discussion of hydrostatic machine feed platform

The thermal deformation of hydrostatic machine feed platform is attributed to the oil film heat transfer towards the platform. The oil output temperatures (T_{out}) of conditions 1–3 are obtained based on the temperature FE results of hydrostatic machine feed platform, respectively. Then, $(T_S+T_{out})/2$ is used to approximately present the average oil film temperature. Furthermore, the temperature gradient between oil films and the environment is:

$$\Delta T = \frac{T_S + T_{out}}{2} - T_A \tag{38}$$

Based on this method above, the time-varying temperature gradients from oil films towards the environment of conditions 1–3 are illustrated and compared in Fig. 15. This figure shows the following: conditions 1–3 have growing temperature gradients with time increase, but the one of condition 2 ($T_A=T_S=20$ °C) is the least and close to 0, compared with the other two conditions. The initial temperature of hydrostatic machine feed platform in operation is generally assumed to be same with ambient temperature. When the hydrostatic machine feed platform is running, the oil film heat transfer is generally through the machine structure and dissipated in the ambient air convection. This heat transfer brings the time-varying machine structure temperature, and this heat transfer is the critical factor causing machine thermal deformation. The heat transfer scale is determined by the temperature gradients from oil films towards the environment. (The negative temperature gradient of condition 3 in Fig. 15 means its reverse heat conveying direction.). Because condition 2 has the least temperature gradient scale, it has the least heat transfer scale to cause machine thermal deformation. This is the reason why the machine thermal deformation in condition 2 is lower than that in the other two conditions, which is presented in Section 3.2. Therefore, condition 2 ($T_A=T_S=20$ °C) is more beneficial than the other two conditions ($T_A<T_S$ and $T_A>T_S$) in cutting down the machine thermal deformation.

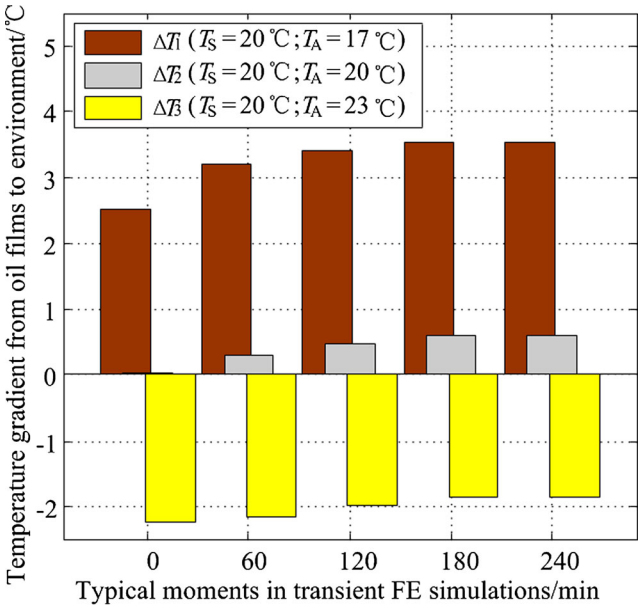

Fig. 15 Time-varying temperature gradients from oil films to environment

5.2 Thermal errors prediction of hydrostatic machine feed platform

5.2.1 Methods for thermal errors prediction of hydrostatic machine feed platform based on FE simulation results

Thermal errors of hydrostatic machine feed platform Δ_Y, Δ_Z, δ_Y, and δ_Z shown in Fig. 5 can be predicted based on its thermal FE simulation results. The prediction method of these thermal errors is introduced, with vertical thermal deformations of hydrostatic machine feed platform in condition 1 being an example: Fig. 16 shows steady vertical thermal deformation values of point O (shown in Fig. 11), when the distance between the slide and the proximal of machine base is 0–1000 mm (increasing step is 200 mm).

These thermal deformations are obtained from the FE simulation results in Section 3.2. As shown in Fig. 16, parallel lines 1 and 2 are located with the minimum distance to include all these thermal deformation values. Then, the straightness error and rotating error of hydrostatic machine feed platform can be predicted [20]. According to the Cartesian coordinate system for hydrostatic machine feed platform in Fig. 5, the distance d of the two parallel lines in Fig. 16 is predicted as Δ_Z, and the angle α caused by two parallel lines with horizontal axis is predicted as δ_Y. They are the predicted thermal errors of hydrostatic machine feed platform.

5.2.2 Machine thermal error variations caused by the temperature gradient from oil film to environment

The method mentioned in Section 5.2.1 can be applied onto the thermal straightness (horizontal and vertical) error and angle error estimations of hydrostatic machine feed platform in condition 1–3. Thus, the influence from quantitative comparison result between T_A and T_S onto thermal errors of

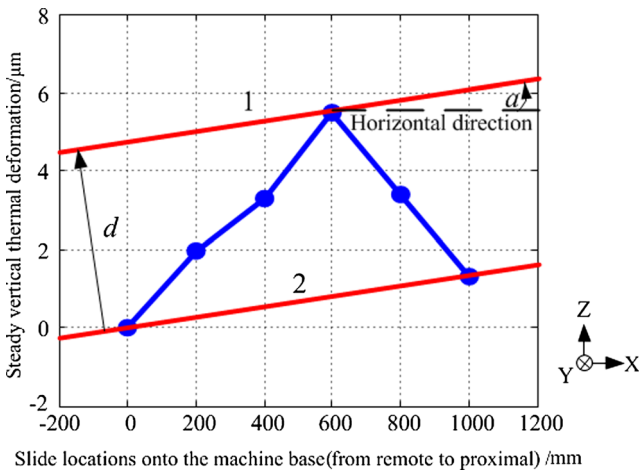

Fig. 16 Thermal straightness error and angle error prediction method of hydrostatic machine feed platform (vertical direction, condition 1)

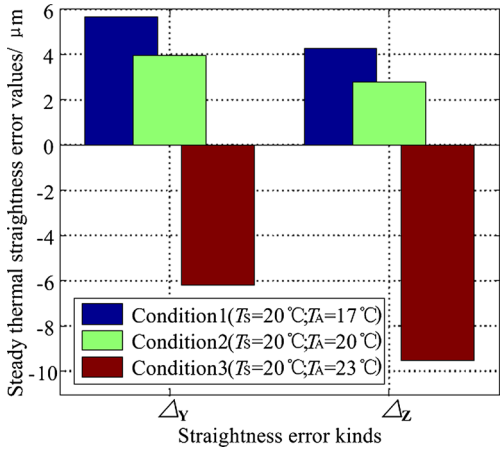

Fig. 17 Comparisons about predicted thermal straightness errors Δ_Y, Δ_Z

hydrostatic machine feed platform can be summarized based on the thermal simulation results of hydrostatic machine feed platform.

Figures 17 and 18 show the comparisons of thermal errors Δ_Y, Δ_Z, δ_Y, and δ_Z in conditions 1–3, based on the prediction method in Section 5.2.1. It can be seen from the comparisons that condition 2 has the smaller thermal straightness errors and angle errors (Δ_Y=3.94 μm, Δ_Z=2.8 μm; δ_Y=−6.3e–007 rad, δ_Z=−3.1333e–007 rad) than the other two conditions because condition 2 has the minimum heat transfer scale through the machine structure in these three conditions. This scale is determined by the temperature gradient from oil films to environment, and the oil film temperature relies on oil supply temperature. Thus, the machine thermal errors are determined by the quantitative comparison result of oil supply temperature and ambient temperature; then, this relative oil supply temperature to ambient temperature should be diminished as possible to reduce machine thermal errors.

Meanwhile, as far as the high- or ultra-precision machine tool are concerned, the desired accuracies of them are generally in the order of micrometer or submicrometer, thermal influence to machine accuracy from the hydrostatic

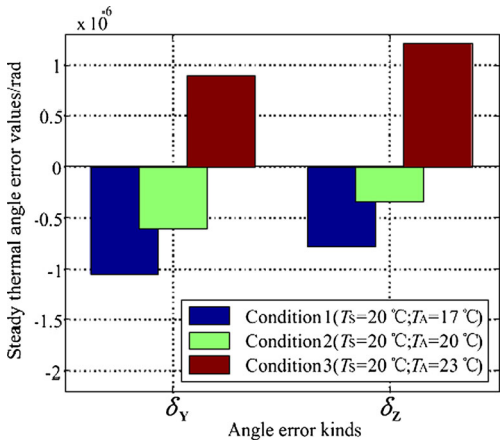

Fig. 18 Comparisons about predicted thermal angle errors δ_Y, δ_Z

guideways cannot be ignored (T_A=T_S=20 °C: Δ_Y=3.94 μm, Δ_Z=2.8 μm; δ_Y=−6.3e−007 rad, δ_Z=−3.1333e−007 rad) and must be taken into the account in design and error compensation about hydrostatic machine tools.

6 Conclusions

A comprehensive thermal simulation modeling method of hydrostatic machine feed platform is presented in this paper, so as to predict its thermal characteristics and study the reducing method of its machine thermal errors. This method includes the theory analyses about the simulation loads of closed hydrostatic guideways and the thermal FE simulation of hydrostatic machine feed platform. Specially, the former is guided by a friction power heat model of viscous hydraulic oil flowing between parallel planes based on Bernoulli equation. The main conclusions of the study are listed as follows:

1. In machine design phase, the presented thermal simulation modeling method of hydrostatic machine feed platform is reliable and accurate to predict and analyze its thermal characteristics, which is verified by experiments.
2. Based on the thermal FE simulation results of the hydrostatic machine feed platform in this paper, machine feed thermal errors Δ_Y, Δ_Z, δ_Y, and δ_Z can be calculated and predicted. For high- or ultra-precision machine tool whose desired accuracy is in the order of micrometer or submicrometer, hydrostatic machine feed errors caused by thermal factors generally cannot be ignored.
3. The hydrostatic machine thermal error degree is determined by the oil film heat transfer scale, and this scale mainly results from the quantitative comparison result of oil supply temperature and ambient temperature. Therefore, the distinction between these two temperatures should be diminished, so as to cut down the oil film heat transfer scale, and then to reduce thermal errors of hydrostatic machine feed platform.

Acknowledgments This paper is supported by the state S&T projects for upmarket NC machine and fundamental manufacturing equipment of China (No. 2014ZX04014-011)

References

1. Wang ZW, Zhao WH, Chen YL, Lu BH (2013) Prediction of the effect of speed on motion errors in hydrostatic guideways. Int J Mach Tools Manuf 64:78–84
2. Xue F, Zhao WH, Chen YL, Wang ZW (2012) Research on error averaging effect of hydrostatic guideways. Precis Eng 36:84–90
3. Yang Z, San AL, Childs DW (1996) Thermal effects in liquid oxygen hydrostatic journal bearings. Tribol Trans 39(3):654–662
4. Sharma SC, Kumar V, Jain SC, Nagaraju T, Prasad G (2002) Thermohydrostatic analysis of slot-entry hybrid journal bearing. Tribol Int 35(9):561–577
5. Sharma SC, Kumar V, Jain SC, Nagaraju T (2003) Study of hole-entry hybrid journal bearing system considering combined influence of thermal and elastic effects. Tribol Int 36(12):903–920
6. Park CH, Oh YJ, Hwang JH, Lee DW (2002) Experimental analysis on thermal characteristics of hydrostatic guideway for precision positioning. 1st Korea Japan Conference of Positioning Technology: 52–57
7. Kumar V, Sharma SC, Jain SC (2004) Stability margin of hybrid journal bearing: influence of thermal and elastic effects. J Tribol - T ASME 126(3):630–634
8. Suzuki H, Urano K, Kumehara H, Kusumoto K (2009) Minimizing thermal deformation of high-precision machine tool induced by hydraulic oil of hydrostatic bearings. Seimitsu Kogaku Kaishi/J Jpn Soc Precis Eng 75(9):1106–1111
9. Kapur VK, Verma K (1979) Simultaneous effects of inertia and temperature on the performance of a hydrostatic thrust bearing. Wear 54(1):113–122
10. Sun GS, Wang ZY, Lu WJ (1992) Research on the temperature field of the hydrostatic and hydrodynamic hybrid bearing. Chin J Mech Eng-En 28(6):74–81
11. Zhang JB, Chi CQ (1997) Analysis of thermal effects in shallow recess-step hydrostatic and hydrodynamic oil bearing. J Beijing Univ Aeronaut and Astronaut 23(3):390–394
12. Zhang GY, Yuan XY (2006) A theoretical study on three-dimensional pressure distributions and temperature field of water-lubricated hydrostatic journal bearings. Lubr Eng 8:4–7
13. Fu YL, Zhu J (2006) Three-dimensional temperature field analysis of hybrid journal bearing. Lubr Eng 2:115–117
14. Chen DJ, Bonis M, Zhang FH, Dong S (2011) Thermal error of a hydrostatic spindle. Precis Eng 35:512–520
15. Jiang Y, Hou GA, Sun T (2011) Thermal finite element analysis of hydrostatic guide. Aviat Precis Manuf Technol 47(5):23–25
16. Wang JH, Du W, Liu ZF, Cai LG (2013) The thermal characteristics analysis of a super hydrostatic guideway. Appl Mech Mater 248:162–166
17. Su H, Lu LH, Liang YC, Zhang Q, Sun YZ (2014) Thermal analysis of the hydrostatic spindle system by the finite volume element method. Int J Adv Manuf Technol 71:1949–1959
18. Wang ZW, Zhao WH, Li BQ, Zhang J, Lu BH (2011) Fluid–structure interactions (FSI) on static characteristics of hydrostatic guideways. 2011 I.E. International Symposium on Assembly and Manufacturing, ISAM 2011
19. Shamoto E, Park CH, Moriwaki T (2001) Analysis and improvement of motion accuracy of hydrostatic feed table. CIRP Ann-Manuf Technol 50(1):285–290
20. Yang JG, Fan KG, Du ZC (2013) Real-time error compensation of CNC machine tools. China machine Press, Beijing
21. Buscaglia GC, Jai M (2004) Homogenization of the generalized Reynolds equation for ultra-thin gas films and its resolution by FEM. J Tribol-T ASME 126:547–552
22. ISO 230-3: 2001, IDT. Test code for machine tools—Part 3: Determination of thermal effects